







Cite this: *Phys. Chem. Chem. Phys.*,
2025, 27, 14815

Exploring quantum tunneling in heavy atom reactions using a rigorous theoretical approach to the dynamics: formation of NO + O from the N + O₂ atmospheric reaction†

Fabrizio Esposito, ^a Pablo Gamallo, ^b Miguel González ^{*b} and Carlo Petrongolo ^c

This theoretical work is centered on the rigorous study of the importance of quantum effects (tunneling and over the barrier reflection (non-classical reflection)) in heavy atom reactions, considering in this case the elementary gas phase reaction $\text{N} + \text{O}_2(v_0 = 0, j_0 = 1) \rightarrow \text{NO} + \text{O}$, which is relevant, e.g., in the oxidation mechanism of nitrogen (Zeldovich's mechanism) and air cold plasmas. We have examined the quantum and classical reaction probability, cross-section (E_{col} : 0.200–0.651 eV) and rate constant (T : 200–1000 K) of this reaction. To do this, we have applied the close-coupling time-dependent real wave packet (CC-TDRWP) method and the quasiclassical trajectory (QCT) method. Even though we are considering a heavy-heavy-heavy atom reactive system, quantum effects are playing a notable role in the low energy region. Thus, for the cross-section they are relevant in the 0.334–0.381 eV E_{col} interval, while below 0.334 eV reactivity is only possible by tunneling (the minimum energy required for $\text{N} + \text{O}_2(v_0 = 0, j_0 = 1)$ to overcome the barrier is 0.299 eV). Furthermore, quantum effects are also evident in the rate constant for temperatures between 200 and 500 K. Lastly, we have also made known the limited degree of validity of the J -shifting approximation in the title reaction. From what we know, this work corresponds to the most rigorous theoretical study carried out so far on quantum effects and reactivity for reactions involving only heavy atoms. We expect that it will encourage more investigations of this type in the future, since it is an interesting problem that has been little explored to date.

Received 10th February 2025,
Accepted 23rd May 2025

DOI: 10.1039/d5cp00539f

rsc.li/pccp

1. Introduction

Around 100 years after the beginning of quantum mechanics, one of the central theories of physics, it continues fascinating both specialists and non-specialists due to the surprising nature of the quantum phenomena, including, e.g., zero-point energy, interferences, resonances and tunneling.^{1,2}

Here, we will mainly focus on the tunneling effect^{3–12} and more specifically on the importance that tunneling presents for the reactivity when a chemical reaction takes place by the transference of a heavy atom (that is, neither a H atom nor

one of its isotopes). In this situation, in general, it has been assumed that this effect is of a small relevance. And, according to this, it has been studied almost exclusively in the framework of the transfer of light or very light species, such as a hydrogen atom or an electron, respectively.

Notwithstanding the above, it is worth keeping in mind that reasonable one-dimensional models show that the barrier width has a stronger influence on the tunneling probability than the height of the barrier and the effective mass of the particles involved.

The tunneling effect is almost always important at low temperatures when the reaction under consideration involves the transfer of light atomic species (H, H⁺ and H[−], mainly). However, this phenomenon can sometimes be also significant in reactions involving the transfer of heavy atomic species (e.g., C, N and O).^{11,14} When the rate constant is considered, in general the larger importance of tunneling in light atom transfer reactions can be interpreted based on the greater (imaginary) frequency of the vibrational normal mode of the transition state that connects reactants and products.

The research activity developed during the recent years in organic chemistry in the context of chemical reactions where

^a Istituto per la Scienza e Tecnologia dei Plasmi, Consiglio Nazionale delle Ricerche, Sede Territoriale di Bari, Via Amendola 122/D, 70126 Bari, Italy

^b Departament de Ciència de Materials i Química Física and Institut de Química Teòrica i Computacional (IQTC), Universitat de Barcelona, Martí i Franquès 1-11, 08028 Barcelona, Spain. E-mail: miguel.gonzalez@ub.edu

^c Istituto per i Processi Chimico Fisici, Consiglio Nazionale delle Ricerche, Via G. Moruzzi 1, 56124 Pisa, Italy

† Electronic supplementary information (ESI) available: Auxiliary figures are included in the ESI document, to mainly provide a more complete view of the reaction probability. See DOI: <https://doi.org/10.1039/d5cp00539f>



heavy atoms, such as, *e.g.*, C, N and O, are those that experience the tunneling effect (see, *e.g.*, ref. 13–23), has been an important stimulus for the development of the present work. Thus, the aforementioned research activity has shown that, in a wide variety of reactions (pericyclic reactions, cycloaromatization, rearrangement of radicals, *etc.*), the tunneling effect involving heavy atoms plays a relevant role.

Given the characteristics (complexity) of these reactions, to estimate theoretically the contribution of the tunneling effect to the reactivity (rate constant) the main approaches used involve one-dimensional models (*i.e.*, those of Wigner, Jeffreys–Wenzel–Kramers–Brillouin (JWKB), Bell, and Truhlar) and the transition state theory (TST) or its variational version (VTST). In the TST or VTST rate constant calculations, carried out using density functional theory (DFT) or *ab initio* information about the reactants and transition state, multidimensional tunneling corrections have been included by means of the zero curvature tunneling (ZCT) or the small curvature tunneling (SCT) corrections.^{10–12} The use of more sophisticated methods is generally not feasible given the significant number of atoms involved in these reactions which, in addition, take place in condensed phase (in solution or in a cryogenic inert gas matrix).

Sometimes the above-mentioned tunneling corrections are confused as being one-dimensional. However, this is not the case as the curvature of the reaction path connecting reactants and products couples the motion along the reaction coordinate with the local vibrational modes that are perpendicular to it (this coupling enters into the Hamiltonian through the kinetic energy term).

It is worth keeping in mind that to determine if a “light atom” or a “heavy atom” tunneling has occurred is not necessarily simple, as light and heavy atoms may be involved simultaneously. In fact, for the barrier defined by the transition state of a given reaction, the normal mode of imaginary frequency usually involves the motion of several atoms. Therefore, the motion of the heavy atom transferred could be accompanied by the motion of one or more light atoms.

Furthermore, it is also worth keeping in mind that while the evolution of the reactants along the minimum energy reaction path (MEP) of the potential energy surface (PES) facilitates the formation of products (after passing over the barrier), this path is not necessarily the best one for reaching products by tunneling.

Concerning the studies of elementary reaction dynamics in which time-independent or time-dependent quantum-mechanical methods have been rigorously applied (*i.e.*, by including the Coriolis coupling (CC)), as far as we know there are only a few cases where reactions with a barrier above reactants and involving a heavy atom transfer have been studied.^{24–30} These reactions involve two heavy atoms and a single light atom: $\text{H} + \text{O}_2 \rightarrow \text{OH} + \text{O}$, $\text{H} + \text{O}_2(a^1\Delta_g) \rightarrow \text{OH} + \text{O}$, $\text{O} + \text{NH} \rightarrow \text{NO} + \text{H}$, $\text{Li} + \text{HF} \rightarrow \text{LiF} + \text{H}$, $\text{Li} + \text{HCl} \rightarrow \text{LiCl} + \text{H}$, and $\text{C}^+ + \text{SH} \rightarrow \text{CS}^+ + \text{H}$. Unfortunately, the influence of tunneling on the reactivity has not been analyzed in any of these six reactions.

Due to the above, here we have focused our attention on the rigorous study of the influence of tunneling on the reactivity of an important heavy atom transfer chemical system. To the best of our knowledge this is the first time that this issue has been considered.

For this purpose, we have selected the $\text{N} + \text{O}_2 \rightarrow \text{NO} + \text{O}$ elementary gas phase reaction ($\Delta_r H_{0K}^0 = -32.09 \text{ kcal mol}^{-1}$),³¹ which is an important chemical process. This reaction is relevant in the Earth's atmospheric chemistry, where it is involved in the oxidation mechanism of nitrogen (Zeldovich's mechanism).³² It corresponds to the second reaction of this mechanism, while the related $\text{O} + \text{N}_2 \rightarrow \text{NO} + \text{N}$ reaction corresponds to the first reaction one.

The study of the kinetics and dynamics of these reactions at high temperature is of particular interest in the context of the physicochemical processes occurring during the re-entry of spacecrafts (hypersonic flight) into the Earth's atmosphere, where the strong nonequilibrium thermal conditions produced play an important role.^{33,34} Under these hard conditions a fraction of the N_2 and O_2 molecules will dissociate and open the way for the production of NO through the Zeldovich's mechanism.

The $\text{N} + \text{O}_2$ reaction is also relevant in shock heated air, supersonic expansion of exhaust gases and combustion processes with hydrocarbon–air mixtures,³⁵ and as a source of infrared chemiluminescence in the upper atmosphere.³⁶ Furthermore, this reaction is also relevant in the context of the air cold plasmas.³⁷

The selected reaction has been the subject of numerous investigations which are mainly of theoretical type. Thus, mostly potential energy surfaces, quasi-classical trajectory and approximate quantum dynamics studies have been developed, considering initially PESs based on a limited number of *ab initio* points,^{38–50} and more recently with higher level PESs.^{51–73} On the other hand, the experimental activity has been mainly focused on the measurement of the rate constant of the reaction⁷⁴ and the vibrational distribution of NO.^{75–79} Besides, crossed molecular beam experiments at high collision energy ($\langle E_{\text{col}} \rangle = 77.5 \text{ kcal mol}^{-1}$) and with the detection of the NO product have been recently reported.⁷¹

In this work we have carried out a rigorous study on the influence of quantum tunneling on the reaction $\text{N} + \text{O}_2 \rightarrow \text{NO} + \text{O}$ taking place on the ground potential energy surface ($1^2A'$ PES), which is, clearly, the most important one at low/moderate temperatures. Moreover, the O_2 molecule is in its lowest energy vibro-rotational state (*i.e.*, $v_0 = 0, j_0 = 1$). For this aim the time-dependent quantum dynamic method based on the propagation of real wave packets has been used, including the Coriolis coupling (see refs. in Section 2). Besides, the quasi-classical trajectory method has been also used (see references in Section 2), and the results obtained with both methods for the probabilities, cross-sections and rate constants have been compared. From this comparison it has been possible to determine the importance of the tunneling effect for the selected properties and its dependence on collision energy and translational temperature.

The article has the following structure: Section 2 briefly presents the theoretical methods and describes the main

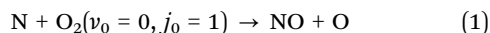


properties of the NO₂ ground potential energy surface; Section 3 reports and discusses the results obtained on the probabilities, cross-sections and rate constants; Section 4 provides the summary and conclusions. Finally, in the ESI,[†] some useful additional information is given.

2. Theoretical methods

2.1. Potential energy surface

The study of the reaction



considering as observables the cross-section and the rate constant, has been performed using quantum and classical methods (see below). In both cases, the well-known and accurate analytical expression of the 1²A' ground PES reported in ref. 52 has been used, which correlates the electronic ground-state of reactants and products. This PES, used together with the first excited 1⁴A' PES,⁵² has allowed achievement of an excellent agreement with experimental data using quasiclassical calculations in a recent work,⁵⁸ in a wide temperature range. The MEP connecting reactants and products has an exoergicity value of ≈ 1.4 eV and includes an early transition state (TS1) located ≈ 0.3 eV above reactants (Table 1). After TS1 there is a shallow minimum (MIN1; ≈ 1.2 eV below reactants) that allows

connecting with NO + O following two different ways: (a) a direct pathway; (b) an indirect pathway that leads to a deep minimum that corresponds to the electronic ground state of the NO₂ molecule [NO₂(\tilde{X}); ≈ 3.3 eV below products] from which products can be formed. This can be seen in Fig. 1.

2.2. Quantum mechanical method

We obtain initial-state-resolved quantum mechanics (QM) reaction probabilities, $P_{j_0 K_0}^J(E_{\text{col}})$, where QM refers to the close-coupling time-dependent real wave packet (CC-TDRWP) method. Thus, we have solved the time dependent Schrödinger equation propagating real wave packets (WPs) up to convergence, and performing a time-to-energy Fourier transform and a flux analysis.^{80,81} We employ reactant Jacobi coordinates: the distance R between N and the O₂ center of mass (CM), the distance r between the O nuclei, and the included angle γ (Fig. 2). Jacobi coordinates are frequently used in many-particle systems to make the mathematical description simpler and are commonly employed in chemical reaction dynamics.⁸² Here J and $p = \pm(-)^J$ label the total angular momentum and parity quantum numbers respectively, j_0 is the O₂ rotational level, $0 \leq K_0 \leq \min(J, j_0)$ is the R -component of both J and j_0 (the body-fixed frame has the z axis pointing along R).

The present quasiclassical trajectory (QCT) method does not resolve p , while uses orbital angular momentum l instead of K_0 ; therefore the comparisons will be of $P_{j_0}^J$ (see below for details), that we have quantum-mechanically calculated considering the J -terms of the integral cross-section,

$$P_{j_0}^J = \left[P_{j_0 0}^{J p_+} + (1 - \delta_{J0}) \sum_{K_0 > 0}^{\min(J, j_0)} \left(P_{j_0 K_0}^{J p_+} + P_{j_0 K_0}^{J p_-} \right) \right] / (2 \min(J, j_0) + 1),$$

$$p_+ = +(-)^J, p_- = -(-)^J \quad (2)$$

Table 1 Properties of the barrier height on the NO₂ ground PES^a

Reactant Jacobi coordinates $R, r, \gamma/a_0$ and deg	4.123, 2.331, 124.6
Energy/eV ^b	0.298
Harmonic vibrational frequencies/cm ⁻¹ ^c	486i, 399, 1221
Energy including ZPE/eV ^b	0.299

^a TS1 transition state.⁵² ^b Energy taken with respect to the N + O₂ reactants. ^c (ν_1, ν_2, ν_3) correspond to the vibrational quantum numbers for the N–O stretching (imaginary frequency), \angle NOO bending, and O–O stretching, respectively.

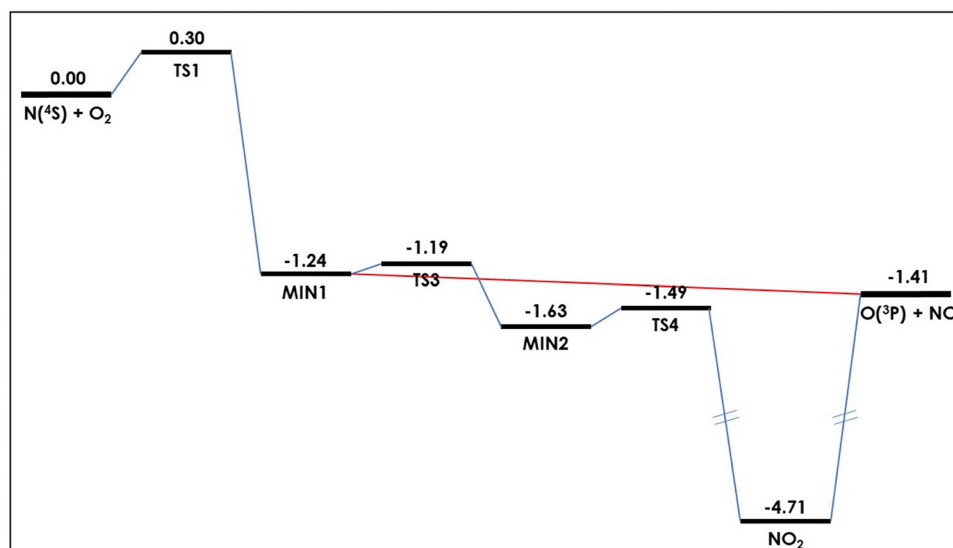


Fig. 1 Schematic representation of the minimum energy path of the (analytical) ground potential energy surface of the N + O₂ → NO + O reaction. Energies are given (in eV) relative to reactants. Data taken from ref. 52.



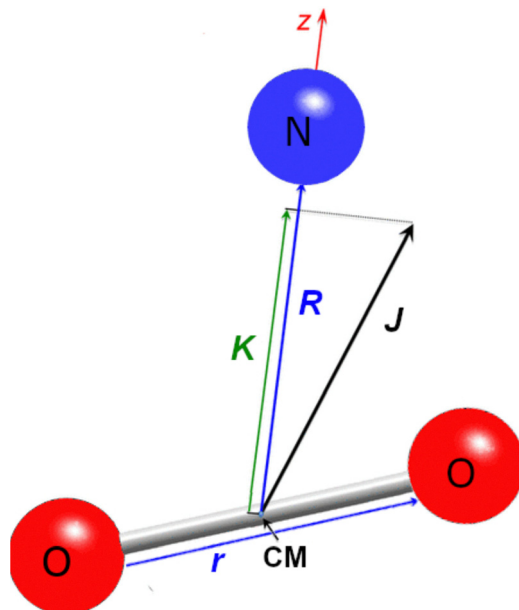


Fig. 2 Reactant Jacobi coordinates of the $\text{N} + \text{O}_2$ system, where the different symbols have the usual meaning (see the text).

QM probabilities are calculated *via* the coupled-channel (CC) method⁸² at $0 \leq J \leq 40$ and $J = 50, 60, 70$ and 90 . Owing to the involved heavy nuclei and the large basis dimensions that are necessary for converging probabilities at high J and E_{col} , we then employed a J -fitting-interpolation technique at the other J s.⁸³ The validity of this approach is reinforced by the fact that the dependence of the reaction probability with E_{col} shows very similar shapes when J is large (the curves for different J s are essentially shifted curves; see also comments below).

We have considered all K components of J along R and the initial WP is defined and propagated *via* the numerical parameters of Table 2. At $J = 0$, we thus employ 7312500 radial-angular basis states, *i.e.* 112500 $|Rr\rangle$ grid states times 65 associated Legendre polynomials $|jK\rangle$, with odd j . These dimensions must be multiplied by $J + 1$ or J according to the two parity values.

Table 2 Parameters of the QM calculations. Values are in a.u., unless otherwise specified

Initial Gaussian $g_0(R)$ [α , E_0 , R_0]	0.15, 0.40 eV, 22
R range and number of grid points	0.0–26 and 450
r range and number of grid points	1.5–10 and 250
Number of $ jK\rangle$	65 with $j \leq 129$
R and r absorption start at ^a	23 and 7
R and r absorption strength ^a	0.01
Flux analysis at r_∞	7
PES and centrifugal energy cut-off	0.44
Number of propagation steps	40 000

^a The expression used for the damping function that removes the wavepacket when it reaches the edges of the system is the following: $\exp[-C_{\text{abs},R}(R - R_{\text{abs}})^2]$ for $R > R_{\text{abs}}$, where $C_{\text{abs},R}$ and R_{abs} correspond to the absorption strength and start, respectively. An analogous expression is applied for the r distance.

The integral cross-section (ICS) for $\text{N} + \text{O}_2(v_0, j_0) \rightarrow \text{NO} + \text{O}$, as a function of E_{col} , and the rate constant (k), as a function of the translational temperature T , are obtained from the following expressions (where v_0 is not indicated):

$$\text{ICS}_{j_0}(E_{\text{col}}) = \frac{\pi \hbar^2}{(2j_0 + 1)2\mu_R E_{\text{col}}} \sum_J (2J + 1) \sum_p^{\min(j_0, J)} \sum_{K_0} P_{j_0 K_0}^{Jp}(E_{\text{col}}) \quad (3)$$

and

$$k_{j_0}(T) = \frac{1}{6} \left(\frac{8}{\pi \mu_R k_B^3 T^3} \right)^{1/2} \times \int_0^\infty E_{\text{col}} \exp(-E_{\text{col}}/k_B T) \text{ICS}_{j_0}(E_{\text{col}}) dE_{\text{col}} \quad (4)$$

where μ_R is the $\text{N} + \text{O}_2$ reduced mass and $1/6$ is the ratio of the electronic degeneracy factors of the transition state (2) and reactants (12) of the PES. The ICS has been studied in the 0.200–0.651 eV E_{col} interval and the rate constant in the 200–1000 K T interval.

2.3. Classical mechanics method

The QCT method was established long ago and is one of the most used theoretical tools for studying chemical reaction dynamics.⁸⁴ The quasiclassical trajectory (QCT) calculations have been performed using standard histogram binning, summing all the final outcomes, *i.e.* including all the possible product vibrational and rotational states. This is exactly equivalent to doing no final state analysis. We proceed in this way because we are interested in total reactivity comparisons, independently of the final states. However, even though the final state analysis is not relevant in this work, we include at the beginning of the ESI† some considerations about final state analysis and tunneling, and a comparison on the use of Gaussian Binning in this context (Fig. S1, ESI†).

The classical dynamics calculations were performed using a variable time step driven by trajectory error analysis.⁸⁵ The typical integration step size used was around 10^{-16} s, with a typical variation of one order of magnitude along each trajectory. The accuracy of the numerical integration of Hamilton's differential equations is verified using the same algorithm governing the time step, because at each step a first integration with time step Δt is compared with two successive calculations with half the previous time step, with tolerance limits on both positions and velocities of 10^{-9} Å and 10^{-9} Å fs⁻¹, respectively. If the test fails, the time step is halved and the cycle is repeated, with a maximum number of attempts equal to 6. This strategy represents an optimal compromise between accuracy and computational load, as tested for different collisional systems (see for example ref. 86).

The trajectories were started at an initial distance of 22 a.u. between the N atom and the center of mass of the O_2 molecule, so that the interaction energy was negligible with respect to the available energy. The same value is adopted for the final distance of interaction. The reaction probability at a given



initial condition (v_0 , j_0 , J , l , and E_{col}) is determined from the number of reactive trajectories obtained divided by the total number of trajectories calculated. This is obtained at fixed quantized values of total and orbital angular momenta, specified by quantum numbers J and l , respectively (see details in equation 7 of ref. 87). This is important in that it allows a direct comparison with QM probabilities, instead of requiring the comparison of complete cross-section calculation, stressing all the possible QCT-QM differences as a function of J . Using this method of QCT calculation, the cross-section is obtained as in eqn (2) for the quantum results, with the only difference being that there is no parity to consider, while K_0 is replaced by the orbital angular momentum quantum number l , which ranges from $|J - j|$ to $J + j$. The sum over l is analogous to the sum over K_0 in eqn (3):

$$P(J) = \left[\sum_{l=|J-j|}^{l=J+j} P(J, l) \right] / (2 \min(J, j_0) + 1). \quad (5)$$

As in the case of the QM calculations, the probabilities are determined at $0 \leq J \leq 40$, $J = 50, 60, 70$ and 90 , and a J -fitting-interpolation technique⁸³ is employed at the other J values.

The total number of trajectories used for the complete calculation of the reaction cross-section from $\text{N} + \text{O}_2(v_0 = 0, j_0 = 1)$ is about 132 million, distributed over a collision energy range from 0.30 to 0.65 eV, uniformly discretized by 0.01 eV (*i.e.*, on average ≈ 3.8 million trajectories are calculated for each collision energy). The lower limit is dictated by the classical threshold imposed by the barrier to reaction and accurately checked by preliminary calculations outside this range. In the vicinity of the reaction threshold, the reaction probability is at least five times the value of its standard error (calculated as usual in QCT), with this happening for probabilities which are just above 10^{-3} . In addition, the probability/standard

error ratio rapidly increases with E_{col} up to two orders of magnitude.

In all the calculations involved in the present work we have used our own CC-TDRWP and QCT computer programs.

3. Results and discussion

In this section the QM and QCT reaction probabilities, cross-sections and rate constants will be presented and the quantum and classical results will be compared and discussed. The contribution of quantum tunneling to the reactivity will be determined for the three properties indicated above.

3.1. QM and QCT reaction probabilities

The reaction probability $P_l(E_{\text{col}})$ as calculated by the QM and QCT methods at fixed J , weighted by the $(2J + 1)$ multiplicative term, and as a function of collision energy is shown in Fig. 3. The factor $(2J + 1)$ makes it possible to compare the weights of different $P(J)$ values in the cross-section calculation, as is clear from equation 3. The general probability trend rapidly increases for all the J considered. Strictly speaking, the exothermic reaction investigated has no threshold energy as the system can evolve from $\text{N} + \text{O}_2$ into $\text{NO} + \text{O}$ without surmounting the energy requirement (barrier and ZPE) associated with the TS1 transition state,⁵² *i.e.*, by leading to products through tunneling. However, the reactivity of the system is extremely small unless the energy of reactants, $E_{\text{col}} + E_{\text{vib-rot}}(\text{O}_2)$, is around/somewhat greater than the energy requirement arising from TS1.

In Fig. 3 it is possible to note the presence of three different regions. In the left panel, the first region is between quantum and classical thresholds (assumed in this figure to be the E_{col} value at which the term $(2J + 1)P(J)$ is equal to 10^{-5}), that are slightly different for each value of J but approximately around 0.23 and 0.35 eV respectively, and where there is a clear

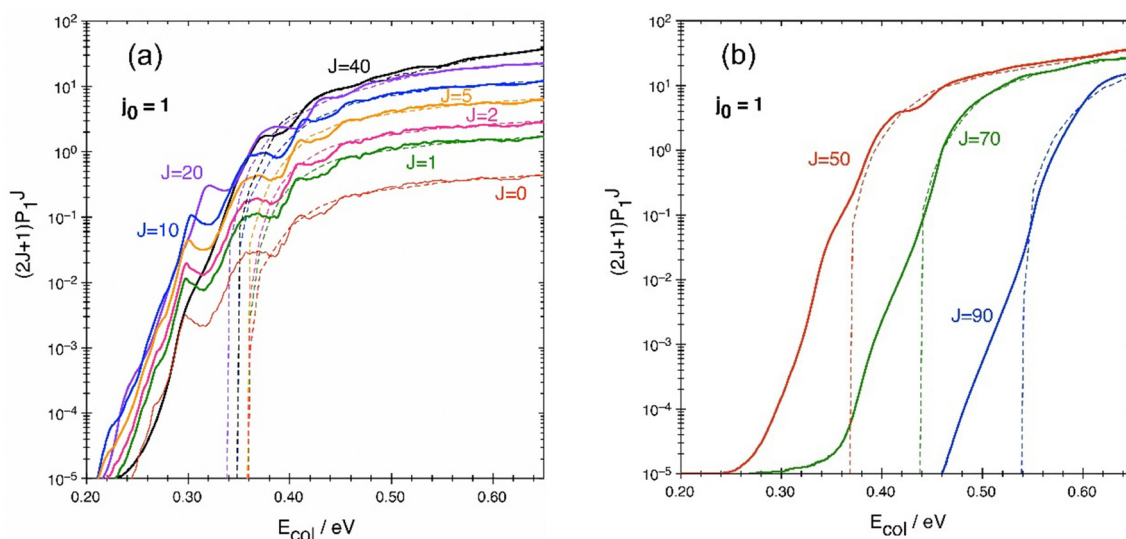


Fig. 3 QM (solid) and QCT (dashed) reaction probabilities for some selected J values between 0 and 40 (a), and between 50 and 90 (b), weighted by the $(2J + 1)$ multiplicative term.



undulatory trend of the quantum probability. The next region is approximately between 0.35 and 0.45 eV, where QCT and QM probabilities are becoming progressively similar, with QM oscillating around the QCT result, which appears as a sort of average of QM probability. In the third region, for collision energies higher than about 0.45 eV the two probabilities are almost coinciding, with only a very weak residual oscillation as a function of collision energy. Interestingly, the oscillations appear to be “in phase” relative to the collision energy for all the probabilities with $0 \leq J \leq 10$. For $J = 20$ the trend is similar but not exactly in phase, while for $J = 40$ some details of the oscillation are lost, and the trend appears to be much smoother (see in particular the smooth trend between 0.30 and 0.35 eV). Similarly to $J = 40$ and differently from the lower J values, the other probabilities for $J = 50, 70$ and 90 in the right panel of Fig. 3 are very smooth, and considering that they are only partially in the second region 0.35–0.45 eV and mostly in the third one, essentially confirm the same features already seen for J values in the left panel, including the level of agreement with QCT results. However, it should be mentioned that the threshold energies for $J = 70$ and 90 are quite larger compared to those for the lower J values.

The considerations that can be made on these results are the following. In the first region, by definition only quantum tunneling is operating. The QM probability peak at about 0.30 eV, common to all the $P(J \leq 10)$, appears to be in perfect accord with the barrier height (see Table 1). However, the way QM trend is much more extended than just around this classical threshold. In fact, it extends practically to the whole energy range explored in this work, with a sort of “damped” oscillation as a function of collision energy. This is reminiscent of the monodimensional quantum tunneling effect of a wavepacket through a rectangular barrier or a well, where an undulatory trend is observed for the transmission coefficient as a function of collision energy. This effect can be rationalized thinking that along the reaction path the collisional system really encounters a small barrier (TS1; 0.299 eV including ZPE) and then one or more wells of different depth, as already commented (see also ref. 52). Of course, in the present three-dimensional case the observed features are much more complex than in a simple monodimensional barrier and very difficult to be put in precise correspondence with the potential energy surface details.

It is interesting to note that the three main peaks in $P(J \leq 10)$ are located at about 0.30, 0.36 and 0.41 eV, values that are quite similar to the energies of the transition state TS1 in the three lowest vibrational levels, 0.299, 0.349 and 0.398 eV, respectively. These vibrational levels, (ν_2, ν_3) , correspond to (0, 0), (1, 0), and (2, 0), respectively (cf. Table 1), and the quantum numbers ν_2 and ν_3 are associated with the vibrational modes involving the \angle NOO bending and O–O stretching, respectively. The N–O stretching mode (quantum number ν_1) is not mentioned above as it is the vibrational mode of imaginary frequency. So, the influence of the quantized vibrational energy levels of TS1 seems to be evident in the probability curves, producing a stepwise evolution of the probability as a function of collision energy.⁸⁸ A detailed study of the transition state control of the reaction as that reported

in ref. 88 for $D + H_2 \rightarrow HD + H$ is out of the scope of the present work.

Approximate expressions for the wave functions corresponding to the (0, 0), (1, 0), and (2, 0) TS1 vibrational levels can be obtained by multiplying the harmonic oscillator 1D vibrational wavefunction of the bending mode normal coordinate (with quantum number equal to 0, 1 or 2) by the corresponding 1D vibrational wavefunction of the O–O stretching mode normal coordinate (with quantum number equal to 0).

Regarding the $(2J + 1)P(J)$ trends of Fig. 3 as a function of collision energy, they follow essentially three different behaviors w.r.t. J . The first behavior is represented by all the $P(J \leq 10)$, in which the same trend in the same energy region is reproduced just by using a multiplicative factor (approximately the $2J + 1$ factor), while no significant energy shifting is needed to approximate one $P(J)$ with another one in the same group, because thresholds are practically the same. The second group is $(2J + 1)P(20 \leq J \leq 40)$, where the trends change significantly with different J values. Some peaks move with J to different positions or disappear. Even in this case, it is quite difficult to see a reliable energy shifting rule in the group. This second group shows the major impact on the cross-section calculation in the second energy region, where $(2J + 1)P(J)$ for lower J are smaller, while higher J contributions are important mainly in the third region. This has significant impact on the QM approximate calculation by J -shifting, as will be clear in the next section. Finally, the third group is $(2J + 1)P(J \geq 50)$ in which the trends are extremely smooth and an energy shifting can easily be used to approximate one trend with $P(J)$ known at another value in the same group. For all intermediate J values not included in this discussion, $(2J + 1)P(J)$ show intermediate behavior w.r.t. the cited groups.

The QM undulatory trend around the QCT result can be clearly appreciated only if probabilities are compared. The effect is much less evident with cross-sections, as will be clear in the next section. In the sum of eqn (3), in fact, most of the oscillations seen in Fig. 3 disappear because the “in phase” oscillations are limited to $P(J \leq 10)$, which have the lowest $(2J + 1)$ weight in the cross-section expression.

Some supporting figures are presented on the reaction probability. Fig. S2 (ESI[†]) presents $(2J + 1)P(J)$ vs. J for a selection of E_{col} offering a complementary view of the results in Fig. 3. Fig. S3 (ESI[†]) shows $P(J)$ vs. E_{col} for a selection of J and also complements Fig. 3 (a similar situation is found in Fig. S4, ESI[†]). Fig. S5 and S6 (ESI[†]) give some insights into the influence of K_0 on the reactivity. Based on the $N + O_2(v_0 = 0, j_0 = 1)$ effective potential energy it can be rationalized why $K_0 = 1$ is more reactive than $K_0 = 0$ (the barrier in the effective potential energy is smaller in the former case). Finally, Fig. S7 (ESI[†]) shows $P(J)$ vs. E_{col} for a selection of j_0 between 1 and 17 ($J = 0, K_0 = 0, p = +$), where in general reactivity increases with O_2 rotational excitation at E_{col} below ≈ 0.4 eV and the results tend to become similar as E_{col} increases.

3.2. QM and QCT reaction cross-sections

The integral cross-sections ICS(QM) and ICS(QCT) are presented in Fig. 4 and Table 3 at the 0.200–0.651 eV E_{col} interval.



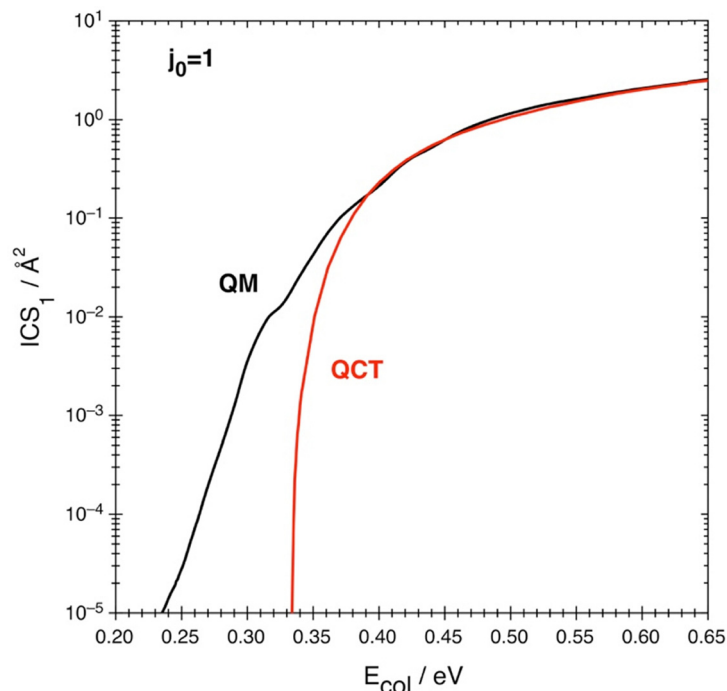


Fig. 4 QM (black) and QCT (red) cross-sections as a function of collision energy.

Table 3 QM and QCT cross-sections and contribution of quantum effects to this property

E_{col}/eV	$\text{ICS}(\text{QM})/\text{\AA}^2$	$\text{ICS}(\text{QCT})/\text{\AA}^2$	$\text{ICS}(\text{QM})/\text{ICS}(\text{QCT})$	Quantum effects contrib./%
0.235 ^a	1.00×10^{-5}			100
0.26	7.20×10^{-5}			100
0.28	4.80×10^{-4}			100
0.3	0.0035			100
0.32	0.0111			100
0.334 ^b	0.0190	1.00×10^{-5}	1900.00	99.95
0.34	0.0262	0.0013	20.15	95.04
0.351	0.0444	0.0101	4.40	77.25
0.361	0.0705	0.0309	2.28	56.17
0.381	0.1341	0.1101	1.22	17.90
0.401	0.2171	0.2365	0.918	-8.94
0.451	0.6359	0.6358	1.00	0.02
0.501	1.1705	1.0770	1.09	7.99
0.551	1.6317	1.5466	1.06	5.22
0.601	2.0773	2.0217	1.03	2.68
0.651	2.5501	2.4756	1.03	2.92

^a Lowest E_{col} at which the QM cross-section is reported ($\text{ICS} = 1.00 \times 10^{-5} \text{\AA}^2$). ^b Lowest E_{col} at which the QCT cross-section is reported ($\text{ICS} = 1.00 \times 10^{-5} \text{\AA}^2$).

They follow a similar behavior, both increasing with E_{col} up to maximum values of 2.55 and 2.48 \AA^2 , respectively, but with the QM reactivity starting at lower E_{col} values. Thus, the lowest value reported here for the ICS ($1.00 \times 10^{-5} \text{\AA}^2$) occurs at $E_{\text{col}} = 0.235$ and 0.334 eV for the ICS(QM) and ICS(QCT), respectively.

These E_{col} are below and above the ZPE-corrected barrier height (0.299 eV) associated with TS1,⁵² respectively, and point out the importance of quantum effects in this energy region (the rotational energy of O_2 in $j_0 = 1$ is very small; 3.58×10^{-4} eV). Therefore, an important contribution of quantum tunneling to

the reactivity is expected to occur below and a little above this energy, justifying the differences observed between the quantum and classical results. We will consider this in detail below.

At the lower E_{col} values, the $\text{ICS}(\text{QM})/\text{ICS}(\text{QCT})$ ratio (Table 3) decreases in a very fast way, varying from 1900 at $E_{\text{col}} = 0.334$ eV to 0.918 at $E_{\text{col}} = 0.401$ eV, with the last value showing the importance of the over the barrier quantum reflection at that collision energy. At higher collision energies this ratio is close or very close to 1.0.

Among all possible processes (reactive and non-reactive) that may occur starting from $\text{N} + \text{O}_2(v_0 = 0, j_0 = 1)$, the $\text{NO} + \text{O}$ reaction channel plays, in general, a minor role in comparison to the inelastic and elastic channels leading to $\text{N} + \text{O}_2$. Thus, for instance, the QM $J = 0$ reaction probability for the $\text{NO} + \text{O}$ channel is below 10% for $E_{\text{col}} \leq 0.408$ eV and reaches values of about 45% only for the higher E_{col} (0.651 eV). Furthermore, at the low collision energies of, e.g., 0.260, 0.280 and 0.299 eV, the reaction probability is only 5.74×10^{-3} , 3.68×10^{-2} and $3.16 \times 10^{-1}\%$, respectively. In spite of these small values, this QM reactivity is essential as at low energies quantum tunneling is the only way to reach the $\text{NO} + \text{O}$ products, accounting for 100% of the reactivity.

For the analysis of the importance of the quantum behavior, we can express the $\text{ICS}(\text{QM})$ as the sum of the $\text{ICS}(\text{QCT})$ and a term that accounts for the quantum correction, $\text{ICS}(\text{QM correction})$, so that we have

$$\text{ICS}(\text{QM}) = \text{ICS}(\text{QCT}) + \text{ICS}(\text{QM correction}) \quad (6)$$

or

$$\text{ICS}(\text{QM correction}) = \text{ICS}(\text{QM}) - \text{ICS}(\text{QCT}) \quad (7)$$



Then, the contribution of the quantum effects to the reactivity of the system (in %), expressed in terms of the ICSs, is given by

$$\begin{aligned} \% \text{quantum effects} &= 100[\text{ICS}(\text{QM correction})/\text{ICS}(\text{QM})] \\ &= 100\{1 - [\text{ICS}(\text{QCT})/\text{ICS}(\text{QM})]\} \end{aligned} \quad (8)$$

Even though, in general, in this context when dealing with quantum effects one often refers to “quantum tunneling”, we have to be aware that the “over the barrier quantum reflection” (non-classical reflection), which leads the system back to the $\text{N} + \text{O}_2$ reactants, is also possible when the total energy of the system is above the ZPE-energy corrected barrier.

The contribution of the quantum effects to the cross-section, expressed according to eqn (8), is not monotonic (Fig. 5 and Table 3) and this differs from what happens in the rate constant (*cf.* Section 3.3), which is a property that involves more averages than the cross-section (*cf.* eqn (4)). Therefore, after a fast decrease of this contribution from $E_{\text{col}} = 0.334$ eV to $E_{\text{col}} = 0.401$ eV (99.95% to -8.94% , respectively), an increase from 0.401 to 0.501 eV (up to 7.99%), a decrease from 0.501 to 0.601 eV (up to 2.68%) and, finally, an increase from the latter collision energy to 0.651 eV (up to 2.92%) follows. With the only exception of the $\approx 0.39\text{--}0.45$ eV E_{col} interval quantum tunneling is more or much more important for the cross-section than the over the barrier quantum reflection. Unfortunately, there is no experimental information available to compare with.

Of course, if the total energy of the system is below the ZPE-corrected barrier height (0.299 eV), this reaction will take place only by quantum effects, whose contribution to reactivity will then be equal to 100%.

The existence of some (small) quantum contribution to the cross-section when the total energy of reactants, $E_{\text{col}} + E_{\text{vib-rot}}[\text{O}_2(v_0 = 0, j_0 = 1)]$, is clearly above the energy of the

barrier (including the ZPE), 0.299 eV, seems reasonable. At a more basic level, we can recall the example of the penetration of a particle through a potential barrier, in which even for collision energy values that are five times the value of the barrier, the quantum effects, although small, are very visible (oscillation of the transmission probability with values that in this case are generally smaller than but close to unity).⁸⁹ Furthermore, the careful convergence tests performed before the production runs, both in the QM and QCT calculations, give confidence regarding the results obtained.

A point of interest in the cross-section context is to compare a widely used approximate method with the accurate QM calculations available now for this collisional system. In Fig. 6 we compare the accurate QM and QCT cross-sections with those obtained from the J -shifting approximation,⁹⁰ used for both QM and QCT. This approximation has been applied as usual considering the specific features of the collisional system, as described *e.g.* in ref. 54 and 64. Therefore, the $P(J)$ values are estimated from the $P(J = 0)$ ones taking into account the rotational energy of the transition state TS1 (described as a nearly prolate symmetric rigid rotor), expressed in terms of J , K_0 and the rotational constants ($A = 2.246 \text{ cm}^{-1}$, $B = 0.330 \text{ cm}^{-1}$ and $C = 0.288 \text{ cm}^{-1}$),

$$P_{j_0 K_0}^J(E_{\text{col}}) \approx P_{j_0 0}^0(E_{\text{col}} - E_{\text{rot}, J K_0}(\text{TS1})) \quad (9)$$

The first observation is that the discrepancy between the accurate and approximate QM calculations is variable but significant along the whole energy axis, with the worst approximation (more than a factor of two) around the energy region between 0.35 and 0.45 eV (the second region in Fig. 3). This coarser approximation is due to the fact that the highest $(2J + 1)P(J)$ values in that region have $20 \leq J \leq 40$, but the

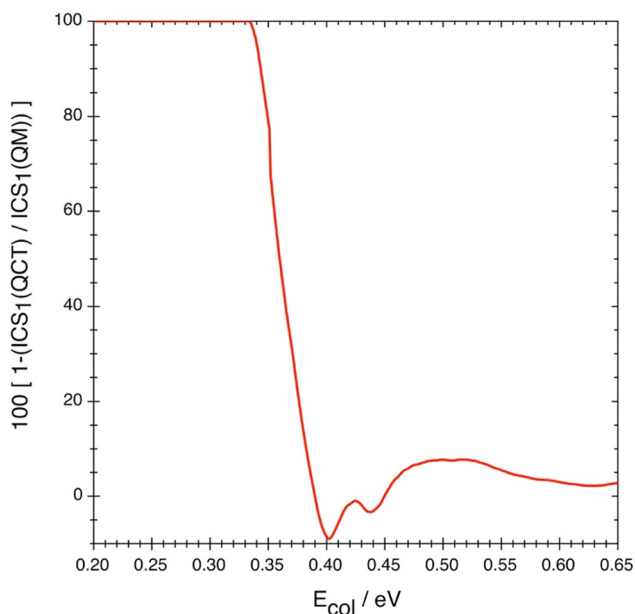


Fig. 5 Contribution of the quantum effects to the cross-section as a function of collision energy.

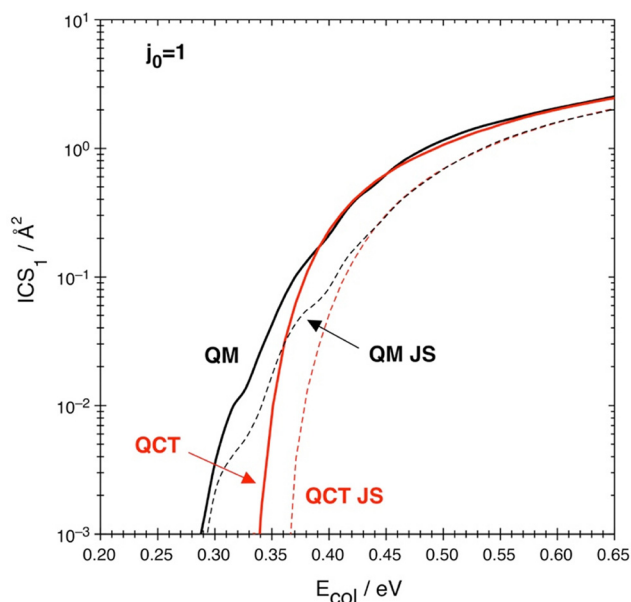


Fig. 6 Quantum (black) and classical (red) cross-sections as obtained without (QCT, QM) and with (QCT JS, QM JS) the J -shifting approximation.



related $P(J)$ are the most difficult to reproduce starting from $P(J=0)$ (see the discussion in the previous section). In contrast, the quality of the results obtained with QCT, with and without the J -shifting approximation, is excellent w.r.t. the appropriate quantum result if considered after a suitable energy threshold. This threshold is about 0.39 eV for accurate QCT and about 0.44 eV for J -shifting QCT. This displacement towards higher values is due to the overemphasizing of the wavy $P(J=0)$ trend in J -shifting w.r.t. the complete calculation including all the J values. This result should be considered when only QM J -shifting calculations are available in comparison with QCT results: an approximate QM calculation is not necessarily better than an accurate QCT one.

The second observation is that the accurate QM cross-section is much smoother than the J -shifting QM result. The undulatory trend of $P(J=0)$ in Fig. 3 heavily reflects in the approximate cross-section curve, but the final effect on the accurate result is just a slight curvature change around $E_{\text{col}} = 0.32$ eV, and another even weaker effect at 0.38 eV.

Another aspect concerning the J -shifting approximation in the present collisional system can be deduced from Fig. 7, where the classical $P(J)$ results are shown, on a linear scale, as a function of E_{col} and for various J values ranging from 0 to 100 (on a linear scale the QM-QCT differences just away from thresholds are much less evident, so for clarity only QCT data are shown here). $P(J=0)$ appears consistently lower than all the other $P(1 \leq J \leq 20)$, with all thresholds quite similar, and the $P(J=0)$ curve shows an opposite curvature w.r.t. any $P(J \geq 30)$. This means that no energy-shift can be used successfully to reproduce all these $P(J > 0)$ using just $P(J=0)$. Only for $J > 40$ this approximation might be applicable starting from $P(J=40)$, as can be easily seen in the threshold displacement along the

energy axis as J increases and the similarity of the $P(J > 40)$ trends.

The present QM and QCT cross-sections for $\text{N} + \text{O}_2(v_0 = 0, j_0 = 1) \rightarrow \text{NO} + \text{O}$ have also been compared with approximate time-dependent (TDRWP)⁵⁵ and time independent⁶⁴ QM results, in which the same analytical expression for the ground PES employed here was used (Fig. S8, ESI†). In these two investigations only the $J = 0$ case was calculated and the cross-sections and rate constants were estimated using the J -shifting approximation. Consistently with the comparison shown in this section between the rigorous and J -shifting results, there are significant differences between the present results and those based on the J -shifting approximation reported in ref. 55 and 64.

3.3. QM and QCT reaction rate constants

The QM and QCT rate constants, $k(\text{QM})$ and $k(\text{QCT})$, respectively, follow the same behavior with both increasing with T , which really corresponds to the translational temperature, as the initial state of O_2 is fixed at $v_0 = 0, j_0 = 1$ (Fig. 8 and Table 4). The two results clearly converge at high temperature. The lowest value reported here for the rate constant occurs at $T = 200$ K, with $k(\text{QM}) = 1.15 \times 10^{-20} \text{ cm}^3 \text{ s}^{-1}$ and $k(\text{QCT}) = 2.61 \times 10^{-21} \text{ cm}^3 \text{ s}^{-1}$. Besides, at the higher temperature explored (1000 K) the rate constants are equal to 1.61×10^{-13} and $1.52 \times 10^{-13} \text{ cm}^3 \text{ s}^{-1}$ for the quantum and classical results, respectively. Therefore, in the 200–1000 K translational temperature interval studied the QM rate constant increases 1.4×10^7 times, while for the QCT results the increment is of 5.8×10^7 times. The larger differences found between the QM and QCT rate constants are observed at the lower temperatures and this results from the differences observed in the ICS at collision energies below ≈ 0.40 eV (see also eqn (4)).

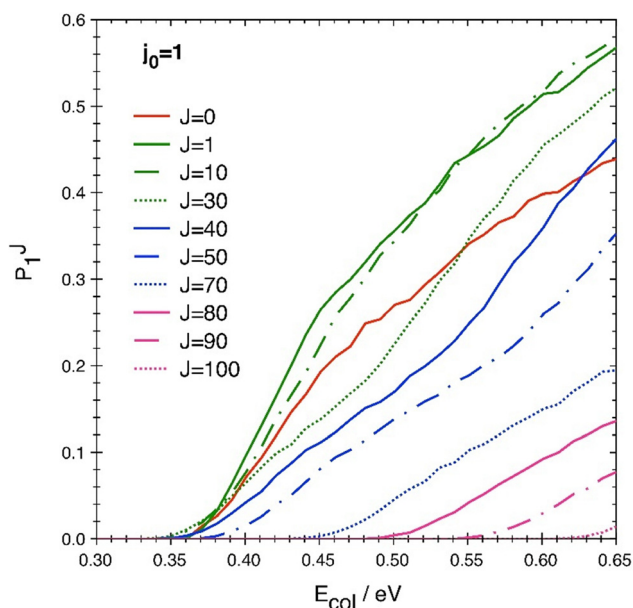


Fig. 7 QCT reaction probability as a function of collision energy for some selected values of J in the 0–100 interval.

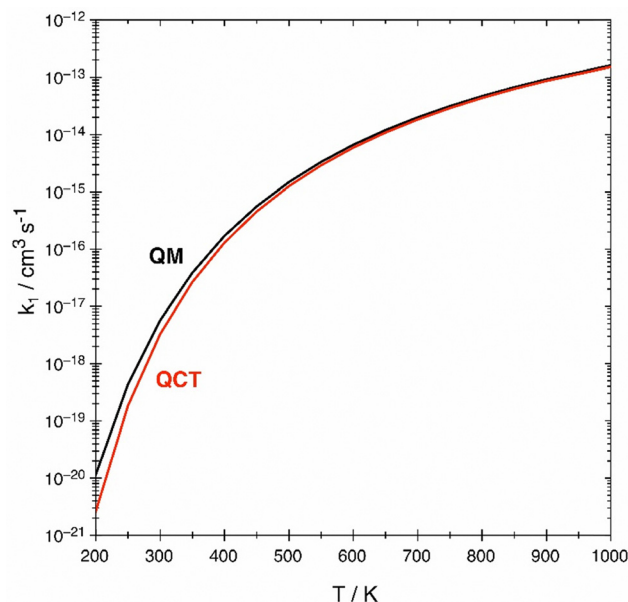


Fig. 8 QM (black) and QCT (red) rate constants as a function of translational temperature.



Table 4 QM and QCT rate constants (in $\text{cm}^3 \text{s}^{-1}$)

T/K	QM	QCT
200	1.15×10^{-20}	2.61×10^{-21}
250	4.39×10^{-19}	1.85×10^{-19}
300	5.73×10^{-18}	3.31×10^{-18}
350	3.89×10^{-17}	2.67×10^{-17}
400	1.71×10^{-16}	1.31×10^{-16}
500	1.49×10^{-15}	1.26×10^{-15}
600	6.65×10^{-15}	5.93×10^{-15}
700	2.01×10^{-14}	1.84×10^{-14}
800	4.72×10^{-14}	4.37×10^{-14}
900	9.29×10^{-14}	8.68×10^{-14}
1000	1.61×10^{-13}	1.52×10^{-13}

The Arrhenius' plot representation ($\ln k$ vs. $1/T$) of the rate constants shows that both $k(\text{QM})$ and $k(\text{QCT})$ exhibit a good linear dependence, *i.e.*, they show Arrhenius' behavior in the 200–1000 K temperature interval (Fig. 9). From this representation the pre-exponential factor, A , and the activation energy, E_a , can be determined. They are shown in Table 5 considering: (a) all data points; (b) the five points of higher T ; (c) the six points of lower T .

The largest differences between the quantum and classical results occur when we compare the Arrhenius' parameters at the lower temperatures (200–500 K), where the $A(\text{QM})/A(\text{QCT})$ and $E_a(\text{QM})/E_a(\text{QCT})$ ratios are equal to 0.433 and 0.899, respectively. In contrast, for the temperature interval 600–1000 K the QM and QCT parameters are very close to each other. This can be rationalized on the basis of the influence of tunneling on the reactivity as it diminishes when temperature grows.

Another way to analyze the differences between the QM and QCT results is based on the $k(\text{QM})/k(\text{QCT})$ ratio, which decreases monotonically with T in the 200–1000 K temperature

Table 5 Arrhenius' parameters A and E_a of the QM and QCT rate constants

T/K		$10^{11}A/\text{cm}^3 \text{s}^{-1}$	E_a/eV
All	QM	0.7399	0.3576
	QCT	1.1057	0.3858
≥ 600	QM	1.8866	0.4119
	QCT	1.9236	0.4187
≤ 500	QM	0.3070	0.3372
	QCT	0.7088	0.3754

interval; with the stronger changes taking place at the lower temperatures. Thus, in the 200–350 K interval defined by the four lower temperatures investigated, the $k(\text{QM})/k(\text{QCT})$ ratio evolves from 4.41 at 200 K to 1.46 at 350 K. Additionally, from 400 to 1000 K the changes in the ratio are small (from 1.31 to 1.06). The larger $k(\text{QM})/k(\text{QCT})$ ratios at the lower T arise from the relevance of quantum tunneling at these temperatures (see below).

Regarding the importance of the quantum behavior in the rate constant and analogously as for the integral cross-section, we can express $k(\text{QM})$ as the sum of $k(\text{QCT})$ and a term that accounts for the quantum correction, $k(\text{QM correction})$, so that we have

$$k(\text{QM}) = k(\text{QCT}) + k(\text{QM correction}) \quad (10)$$

or

$$k(\text{QM correction}) = k(\text{QM}) - k(\text{QCT}) \quad (11)$$

Then, the contribution of quantum effects (quantum tunneling and over the barrier reflection (non-classical reflection)) to the reactivity of the system, expressed in terms of the rate constants, will be given, in %, by

$$\begin{aligned} \% \text{quantum effects} &= 100[k(\text{QM correction})/k(\text{QM})] \\ &= 100\{1 - [k(\text{QCT})/k(\text{QM})]\} \end{aligned} \quad (12)$$

The dependence of the contribution of quantum effects to the reactivity with respect to temperature, determined from equation 12, is a monotonically decreasing function (Fig. 10). This differs from the ICS that shows a non-monotonic dependence with E_{col} , as previously indicated. From 200 to 500 K, the contribution of quantum effects (dominated by tunneling) to the reactivity changes from 77.3% to 15.4%, respectively. And at the two higher temperatures reported (900 and 1000 K) the contribution is of 6.6 and 5.6%, respectively. The higher quantum contribution to reactivity at the lower temperatures is expected, since in this situation the lower E_{col} values have a stronger influence on the rate constant than at higher temperatures.

As in the case of the integral cross-section, it is not possible to compare with experimental information on the $\text{N} + \text{O}_2(v_0 = 0, j_0 = 1) \rightarrow \text{NO} + \text{O}$ rate constant. However, a variational transition state theory analysis, including an estimation of tunneling using a multidimensional approach (the ICVT/ μOMT method), suggested a tunneling contribution of 21.3% (μOMT quantum transmission coefficient = 1.27) for the $\text{N} + \text{O}_2 \rightarrow \text{NO} + \text{O}$ rate

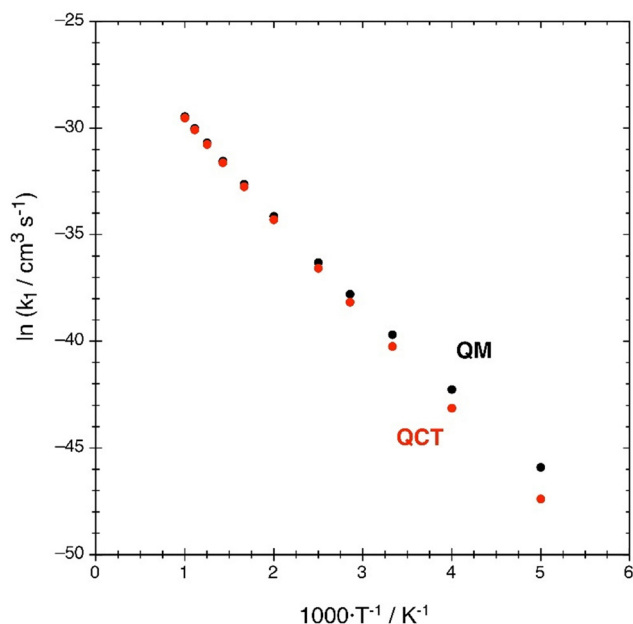


Fig. 9 Arrhenius' plots of the QM (black) and QCT (red) rate constants, with k_1 in $\text{cm}^3 \text{s}^{-1}$ and T in K.



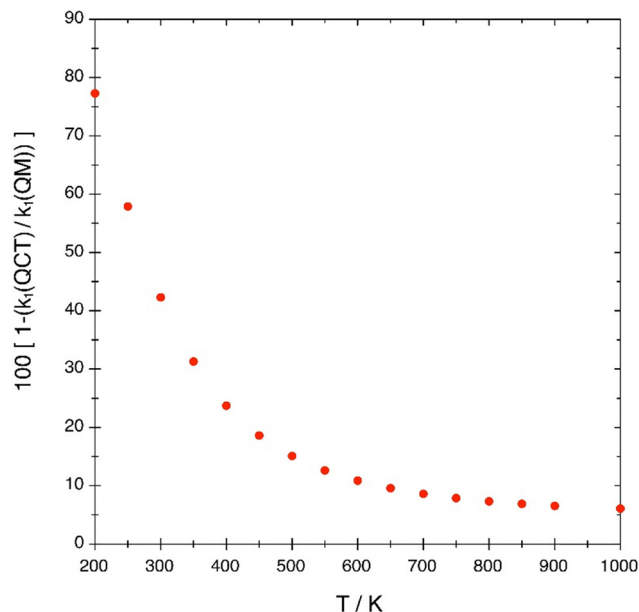


Fig. 10 Quantum contribution to the rate constant as a function of translational temperature.

constant at $T = 300$ K.⁵² It should be highlighted that the ICVT/ μ OMT study mentioned was carried out employing the same analytical expression for the ground potential energy surface of the NO_2 system used in the present work. The first excited ($1^4\text{A}'$) NO_2 PES, that was also considered in ref. 52, has a completely negligible contribution to the rate constant at 300 K.

At the temperature of 300 K, the $\text{N} + \text{O}_2(v_0 = 0, j_0 = 1) \rightarrow \text{NO} + \text{O}$ state specific reaction investigated presents a quantum contribution (dominated by tunneling) of 42.2% in its rate constant. Even though this value is of the order of magnitude of the value estimated by the ICVT/ μ OMT method, it must be emphasized that the reaction conditions are different, as in this last calculation⁵² the O_2 molecule presents a 300 K Boltzmann distribution, which mainly consists in $v_0 = 0$ and several j_0 levels (1, 3, 5, ...). For completeness, the logarithmic plots of the $k(v_0 = 0, j_0 = 1, T)$ and $k(T)$ rate constants vs. T are shown in Fig. S9 of the ESI,[†] where it can be seen that the shapes are similar but the last one presents higher values.

4. Summary and conclusions

This theoretical work has mainly focused on the rigorous study of the importance of quantum effects in heavy atom reactions, considering in this initial investigation the elementary tri-atomic reaction $\text{N} + \text{O}_2(v_0 = 0, j_0 = 1) \rightarrow \text{NO} + \text{O}$. This reaction, which involves three heavy atoms, is very relevant in atmospheric chemistry (Zeldovich's mechanism) and is also important in air cold plasmas. We have studied the dynamics at an exact (close coupling) quantum mechanical level, using the time-dependent real WP method, and at the classical mechanics level using the QCT method; and we have determined the reaction probability, cross-section (E_{col} interval: 0.200–0.651 eV) and rate constant (T interval: 200–1000 K).

The dependence of the reaction probability and reaction cross-section on the collision energy shows the characteristic shape of reactions that present a barrier between reactants and products, both for quantum and classical results. Thus, on the overall, both properties increase with E_{col} and tend to become constant at high enough E_{col} values (but not too high E_{col} so as to open other reaction channels, e.g., the $\text{N} + \text{O} + \text{O}$ dissociation). Regarding the rate constant, it shows a dependence of Arrhenius' type also in both cases.

For the conditions in which the total energy of reactants, $E_{\text{col}} + E_{\text{vib-rot}}[\text{O}_2(v_0 = 0, j_0 = 1)]$, is lower than the energy of the barrier (including the ZPE), 0.299 eV, the $\text{NO} + \text{O}$ production is only possible thanks to the quantum tunneling effect.

When the total energy of the reactants is slightly higher than the energy requirement indicated above, the contribution to reactivity due to the quantum tunneling effect is dominant. Thus, for example, the $\text{ICS}(\text{QM})/\text{ICS}(\text{QCT})$ ratio evolves from a value of 1900 at $E_{\text{col}} = 0.334$ eV to 2.28 at $E_{\text{col}} = 0.361$ eV, and it is not far from unity for 0.381 eV (1.22). At this point, it is worth keeping in mind that for $E_{\text{col}} = 0.361$ eV the total energy of the system is only 0.062 eV (1.43 kcal mol⁻¹) above the energy requirement. At higher E_{col} energies, the minimum value for the $\text{ICS}(\text{QM})/\text{ICS}(\text{QCT})$ ratio (0.92) is obtained at $E_{\text{col}} = 0.401$ eV, i.e., at this energy the quantum reflection over the barrier (non-classical reflection) is more important than quantum tunneling. Moreover, in the 0.551–0.651 eV collision energy range the ratio is basically constant and equal to 1.05.

The $k(\text{QM})/k(\text{QCT})$ rate constant ratio evolves from a value of 4.41 at 200 K to a value of 1.31 at 400 K. Quantum effects are very significant in the temperature range 200–400 K with tunneling being the most important one. Besides, this rate constant ratio decreases progressively from 1.18 at 500 K to 1.06 at 1000 K.

Based on the present results, we can conclude that in this heavy-heavy-heavy atom reactive system quantum tunneling is very important for the ICS in the E_{col} range 0.334–0.381 eV. Besides, below 0.334 eV the reactivity is, essentially, only possible due to the quantum tunneling effect. Quantum effects on the reactivity also manifest significantly in the rate constant between 200 and 500 K.

Finally, we have also shown the limited degree of validity of the J -shifting approximation when applied to determine the cross-section of the selected reaction, from both the quantum and classical perspectives.

To the best of our knowledge, this work is the most rigorous and detailed theoretical study carried out to date on the tunneling effect (and, more generally, on quantum effects and reactivity) in the context of reactions involving only heavy atoms. We hope that this work will be a stimulus for more investigations about this interesting problem to be developed in the future.

Data availability

The data supporting the findings of this study are available from the authors upon reasonable request.



Conflicts of interest

There are no conflicts of interest to declare.

Acknowledgements

This work has been supported by the Spanish Ministry of Science and Innovation (Excellence MDM CEX2021-001202-M). Moreover, some support has also been provided by the Autonomous Government of Catalonia (2021SGR 00354 and 2021SGR 00079 Projects). We are also very grateful to A. Bernini and M. Olivucci for invaluable computing resources provided and to R. A. Sultanov and N. Balakrishnan for sharing with us their $\text{N} + \text{O}_2(v_0 = 0, j_0 = 1)$ reaction probabilities for $J = 0$. This article is dedicated to Professor Donald G. Truhlar (University of Minnesota) for his very important contributions in reaction dynamics and, in particular, for the study of the tunneling effect in chemical reactions.

References

- 1 R. P. Feynman, R. B. Leighton and M. Sands, *The Feynman Lectures on Physics, (Quantum Mechanics)*, Basic Books, New York, 2010, vol. 3.
- 2 C. Cohen-Tannoudji, B. Diu and F. Laloë, *Mécanique Quantique*, EDP/CNRS, Paris, 2018.
- 3 C. Eckart, The penetration of a potential barrier by electrons, *Phys. Rev.*, 1930, **35**, 1303–1309.
- 4 E. P. Wigner, Über das überschreiten von potentialschwellen bei chemischen reaktionen, *Z. Phys. Chem.*, 1932, **B19**, 203–216.
- 5 R. P. Bell, The tunnel effect correction for parabolic potential barriers, *Trans. Faraday Soc.*, 1959, **55**, 1–4.
- 6 B. C. Garrett and D. G. Truhlar, Accuracy of tunneling corrections to transition state theory for thermal rate constants of atom transfer reactions, *J. Phys. Chem.*, 1979, **83**, 200–203.
- 7 R. P. Bell, *The Tunnel Effect in Chemistry*, Chapman and Hall, London, 1980.
- 8 J. Singh, *Quantum Mechanics: Fundamentals and Applications to Technology*, John-Wiley and Sons, New York, 1997, pp. 126–169.
- 9 M. Razavy, *Quantum Theory of Tunneling*, World Scientific, New Jersey, 2003.
- 10 A. Fernandez-Ramos, B. A. Ellingson, B. C. Garrett and D. G. Truhlar, Variational transition state theory with multidimensional tunneling, *Rev. Comput. Chem.*, 2007, **23**, 125–232.
- 11 J. L. Bao and D. G. Truhlar, Variational transition state theory: theoretical framework and recent developments, *Chem. Soc. Rev.*, 2017, **46**, 7548–7596.
- 12 D. G. Truhlar, Semiclassical multidimensional tunneling calculations, in *Tunnelling in Molecules: Nuclear Quantum Effects from Bio to Physical Chemistry*, ed. J. Kaestner and S. Kozuch, RSC Publishing, Cambridge, 2021, pp. 261–282.
- 13 W. T. Borden, Reactions that involve tunneling by carbon and the role that calculations have played in their study, *Wiley Interdiscip. Rev.: Comput. Mol. Sci.*, 2016, **6**, 20–46.
- 14 J. Meisner and J. Kästner, Atom tunneling in Chemistry, *Angew. Chem., Int. Ed.*, 2016, **55**, 5400–5413.
- 15 T. Schleif, J. Mieres-Perez, S. Henkel, M. Ertelt, W. T. Borden and W. Sander, The Cope rearrangement of 1,5-dimethyl-semibullvalene-2(4)-d1: experimental evidence for heavy-atom tunneling, *Angew. Chem., Int. Ed.*, 2017, **56**, 10746–10749.
- 16 C. Doubleday, R. Armas, D. Walker, C. V. Cosgriff and E. M. Greer, Heavy-atom tunneling calculations in thirteen organic reactions: tunneling contributions are substantial, and Bell's formula closely approximates multidimensional tunneling at ≥ 250 K, *Angew. Chem., Int. Ed.*, 2017, **56**, 13099–13102.
- 17 C. M. Nunes, A. K. Eckhardt, I. Reva, R. Fausto and P. R. Schreiner, Competitive nitrogen versus carbon tunneling, *J. Am. Chem. Soc.*, 2019, **141**, 14340–14348.
- 18 C. Castro and W. L. Karney, Heavy-atom tunneling in organic reactions, *Angew. Chem., Int. Ed.*, 2020, **59**, 8355–8366.
- 19 S. Karkamar and A. Datta, Heavy-atom tunneling in organic transformations, *J. Chem. Sci.*, 2020, **132**, 127.
- 20 T. Schleif, M. Prado Merini, S. Henkel and W. Sander, Solvation effects on quantum tunneling reactions, *Acc. Chem. Res.*, 2022, **55**, 2180–2190.
- 21 T. Schleif, Transformations of strained three-membered rings a common, yet overlooked, motif in heavy-atom tunneling reactions, *Chem. – Eur. J.*, 2022, **28**, e202201775.
- 22 J. F. Rowen, F. Beyer, T. Schleif and W. Sander, Isomer-specific heavy-atom tunneling in the ring expansion of fluorenylazirines, *J. Org. Chem.*, 2023, **88**, 7893–7900.
- 23 W. Guo, E. E. Robinson, R. J. Thomson and D. J. Tantillo, Heavy atom quantum mechanical tunneling in total synthesis, *Org. Lett.*, 2024, **26**, 4606–4609.
- 24 P. Honvault, S. Y. Lin, D. Xie and H. Guo, Differential and integral cross sections for the $\text{H} + \text{O}_2 \rightarrow \text{OH} + \text{O}$ combustion reaction, *J. Phys. Chem. A*, 2007, **111**, 5349–5352.
- 25 J. Ma, H. Guo, C. Xie, A. Lib and D. Xie, State-to-state quantum dynamics of the $\text{H}(^2\text{S}) + \text{O}_2(\text{a}^1\Delta_g) \rightarrow \text{O}(^3\text{P}) + \text{OH}(^2\Pi)$ reaction on the first excited state of $\text{HO}_2(\text{A}^2\text{A}')$, *Phys. Chem. Chem. Phys.*, 2011, **13**, 8407–8413.
- 26 A. Li, C. Xie, D. Xie and H. Guo, State-to-state quantum dynamics of the $\text{O}(^3\text{P}) + \text{NH}(X^3\Sigma^-)$ reaction on the three lowest-lying electronic states of HNO/HON , *J. Chem. Phys.*, 2013, **138**, 024308.
- 27 H. Guo, J. Ma and J. Li, Tunneling in unimolecular and bimolecular reactions, in *Molecular Quantum Dynamics. From Theory to Applications*, ed. F. Gatti, Springer, Berlin, 2014, pp. 59–80.
- 28 J. Hazra and N. Balakrishnan, Quantum dynamics of tunneling dominated reactions at low temperatures, *New J. Phys.*, 2015, **17**, 055027.
- 29 L. Zhang, J. Zhao, D. Liu, W. Wang, D. Yue, Y. Song and Q. Meng, A new global analytical *ab initio* potential energy surface for the dynamics of the $\text{C}^+(^2\text{P}) + \text{SH}(X^2\Pi)$ reaction, *Phys. Chem. Chem. Phys.*, 2022, **24**, 1007–1015.



- 30 S. Y. Kumar and R. Padmanaban, Dynamical and mechanical insights into the $\text{Li}(^2\text{S}) + \text{HCl}(\text{X}^1\Sigma^+)$ reaction: a detailed quantum wavepacket study, *ChemPhysChem*, 2023, **24**, e202200747.
- 31 M. W. Chase, Jr., C. A. Davies, J. R. Downey, Jr., D. J. Frurip, R. A. McDonald and A. N. Syverud, *J. Phys. Chem. Ref. Data*, 1985, **14**(Supplement No. 1).
- 32 Y. B. Zeldovich, The oxidation of nitrogen in combustion explosions, *Acta Physicochim. USSR*, 1946, **21**, 577–628.
- 33 S. B. Brooks, M. J. Lewis and R. R. Dickerson, Nitric oxide emissions from the high-temperature viscous boundary layers of hypersonic aircraft within the stratosphere, *J. Geophys. Res.*, 1993, **98**, 16755–16760.
- 34 G. Colonna, F. Bonelli and G. Pascasio, Impact of fundamental molecular kinetics on macroscopic properties of high-enthalpy flows: the case of hypersonic atmospheric entry, *Phys. Rev. Fluids*, 2019, **4**, 033404.
- 35 A. Burcat, G. Dixon-Lewis, M. Frenklach, W. C. Gardiner, R. K. Hanson, S. Salimian, J. Troe, J. Warnatz and R. Zellner, in *Combustion Chemistry*, ed. W. C. Gardiner, Jr., Springer-Verlag, New York, 1984.
- 36 P. Warneck, *Chemistry of the Natural Atmosphere*, Academic, San Diego, 1998, ch. 3.
- 37 F. Esposito, On the relevance of accurate input data for vibrational kinetics in air cold plasmas: the case of nitrogen fixation, *Plasma Sources Sci. Technol.*, 2022, **31**, 094010.
- 38 S. P. Walch and R. L. Jaffe, Calculated potential surfaces for the reactions: $\text{O} + \text{N}_2 \rightarrow \text{NO} + \text{N}$ and $\text{N} + \text{O}_2 \rightarrow \text{NO} + \text{O}$, *J. Chem. Phys.*, 1987, **86**, 6946–6956 and references cited therein.
- 39 R. L. Jaffe, M. D. Pattengill and D. W. Schwenke, Classical trajectory studies of gas phase reaction dynamics and kinetics using *ab initio* potential energy surfaces, in *Supercomputer Algorithms for Reactivity, Dynamics and Kinetics of Small Molecules*, ed. A. Laganà, Kluwer, Dordrecht, 1989, pp. 367–382.
- 40 M. Gilibert, A. Aguilar, M. González and R. Sayós, Quasi-classical trajectory study of the $\text{N}(^4\text{S}_u) + \text{O}_2(\text{X}^3\Sigma_g^-) \rightarrow \text{NO}(\text{X}^2\Pi) + \text{O}(^3\text{P}_g)$ atmospheric reaction on the $^2\text{A}'$ ground potential energy surface employing an analytical Sorbie-Murrell potential, *Chem. Phys.*, 1993, **172**, 99–115.
- 41 M. Gilibert, A. Aguilar, M. González and R. Sayós, A quasi-classical trajectory study of the effect of the initial rovibrational level and relative translational energy of reactants on the dynamics of the $\text{N}(^4\text{S}_u) + \text{O}_2(\text{X}^3\Sigma_g^-) \rightarrow \text{NO}(\text{X}^2\Pi) + \text{O}(^3\text{P}_g)$ atmospheric reaction on the $^2\text{A}'$ ground potential energy surface, *Chem. Phys.*, 1993, **178**, 287–303.
- 42 R. Sayós, A. Aguilar, M. Gilibert and M. González, Orientational dependence of the $\text{N}(^4\text{S}) + \text{NO}(\text{X}^2\Pi)$ and $\text{N}(^4\text{S}) + \text{O}_2(\text{X}^3\Sigma_g^-)$ reactions: comparison of the angle-dependent line-of-centres model with quasiclassical trajectories, *J. Chem. Soc., Faraday Trans.*, 1993, **89**, 3223–3234.
- 43 M. Gilibert, X. Giménez, M. González, R. Sayós and A. Aguilar, A comparison between experimental, quantum and quasiclassical properties for the $\text{N}(^4\text{S}_u) + \text{O}_2(\text{X}^3\Sigma_g^-) \rightarrow \text{NO}(\text{X}^2\Pi) + \text{O}(^3\text{P}_g)$ reaction, *Chem. Phys.*, 1995, **191**, 1–15.
- 44 R. Sayós, J. Hijazo, M. Gilibert and M. González, Variational transition state calculation of the rate constants for the $\text{N}(^4\text{S}_u) + \text{O}_2(\text{X}^3\Sigma_g^-) \rightarrow \text{NO}(\text{X}^2\Pi) + \text{O}(^3\text{P}_g)$ reaction and its reverse between 300 and 5000 K, *Chem. Phys. Lett.*, 1998, **284**, 101–108.
- 45 R. D. Sharma, Y. Sun and A. Dalgarno, Highly rotationally excited nitric oxide in the terrestrial thermosphere, *Geophys. Res. Lett.*, 1993, **20**, 2043–2045.
- 46 N. Balakrishnan and A. Dalgarno, Rate coefficients for NO formation in energetic $\text{N} + \text{O}_2$ collisions, *Chem. Phys. Lett.*, 1999, **302**, 485–488.
- 47 B. Ramachandran, N. Balakrishnan and A. Dalgarno, Vibrational-rotational distributions of NO formed from $\text{N} + \text{O}_2$ reactive collision, *Chem. Phys. Lett.*, 2000, **332**, 562–568.
- 48 J. W. Duff, F. Bien and D. E. Paulsen, Classical dynamics of $\text{N}(^4\text{S}) + \text{O}_2(\text{X}^3\Sigma_g^-) \rightarrow \text{NO}(\text{X}^2\Pi) + \text{O}(^3\text{P})$ reaction, *Geophys. Res. Lett.*, 1994, **21**, 2043–2046.
- 49 G. Suzzi Valli, R. Orrú, E. Clementi, A. Laganà and S. Crocchianti, Rate coefficients for the $\text{N} + \text{O}_2$ reaction computed on an *ab initio* potential energy surface, *J. Chem. Phys.*, 1995, **102**, 2825–2832.
- 50 D. Bose and G. V. Candler, Thermal rate constants of the $\text{O}_2 + \text{N} \rightarrow \text{NO} + \text{O}$ reaction based on the $^2\text{A}'$ and $^4\text{A}'$ potential-energy surfaces, *J. Chem. Phys.*, 1997, **107**, 6136–6145.
- 51 R. Sayós, C. Oliva and M. González, The lowest doublet and quartet potential energy surfaces involved in the $\text{N}(^4\text{S}) + \text{O}_2$ reaction. I. *Ab initio* study of the C_s -symmetry ($^2\text{A}'$, $^4\text{A}'$) abstraction and insertion mechanisms, *J. Chem. Phys.*, 2001, **115**, 1287–1297.
- 52 R. Sayós, C. Oliva and M. González, New analytical $^2\text{A}'$, $^4\text{A}'$ surfaces and theoretical rate constants for the $\text{N}(^4\text{S}) + \text{O}_2$ reaction, *J. Chem. Phys.*, 2002, **117**, 670–679.
- 53 M. González, C. Oliva and R. Sayós, The lowest doublet and quartet potential energy surfaces involved in the $\text{N}(^4\text{S}) + \text{O}_2$ reaction. II. *Ab initio* study of the C_{2v} -symmetry insertion mechanism, *J. Chem. Phys.*, 2002, **117**, 680–692.
- 54 P. Defazio, C. Petrongolo, S. K. Gray and C. Oliva, Wave packet dynamics of the $\text{N}(^4\text{S}_u) + \text{O}_2(\text{X}^3\Sigma_g^-) \rightarrow \text{NO}(\text{X}^2\Pi) + \text{O}(^3\text{P}_g)$ reaction on the $\text{X}^2\text{A}'$ potential energy surface, *J. Chem. Phys.*, 2001, **115**, 3208–3214.
- 55 P. Defazio, C. Petrongolo, C. Oliva, M. González and R. Sayós, Quantum dynamics of the $\text{N}(^4\text{S}) + \text{O}_2$ reaction on the $\text{X}^2\text{A}'$ and $\text{a}^4\text{A}'$ surfaces: reaction probabilities, cross sections, rate constants, and product distributions, *J. Chem. Phys.*, 2002, **117**, 3647–3655.
- 56 P. Defazio, S. Akpınar and C. Petrongolo, Quantum calculations of nonadiabatic $^2\text{A}_1$ – $^2\text{B}_2$ conical-intersection effects in the reactions $\text{N}(^4\text{S}) + \text{O}_2(\text{X}^3\Sigma_g^-)$ and $\text{N}(^4\text{S}) + \text{O}_2(\text{A}^3\Delta_u)$, *Chem. Phys.*, 2010, **375**, 46–51.
- 57 I. Armenise and F. Esposito, $\text{N} + \text{O}_2(v)$ collisions: reactive, inelastic and dissociation rates for state-to-state vibrational kinetic models, *Chem. Phys.*, 2021, **551**, 111325.
- 58 F. Esposito and I. Armenise, Reactive, inelastic, and dissociation processes in collisions of atomic nitrogen with molecular oxygen, *J. Phys. Chem. A*, 2021, **125**, 3953–3964.



- 59 I. Armenise, Low temperature state-to-state vibrational kinetics of $O + N_2(v)$ and $N + O_2(v)$ collisions, *Chem. Phys.*, 2023, **571**, 111937.
- 60 A. J. C. Varandas, A realistic multi-sheeted potential energy surface for $NO_2(^2A')$ from the double many-body expansion method and a novel multiple energy-switching scheme, *J. Chem. Phys.*, 2003, **119**, 2596–2613.
- 61 P. J. B. S. Caridade and A. J. C. Varandas, Dynamics study of the $N(^4S) + O_2$ reaction and its reverse, *J. Phys. Chem. A*, 2004, **108**, 3556–3564.
- 62 V. C. Mota, P. J. S. B. Caridade and A. J. C. Varandas, *Ab initio*-based global double many-body expansion potential energy surface for the first $^2A''$ electronic state of NO_2 , *J. Phys. Chem. A*, 2012, **116**, 3023–3034.
- 63 V. Kurkal, P. Fleurat-Lessard and R. Schinke, NO_2 : global potential energy surfaces of the ground and the first excited electronic states, *J. Chem. Phys.*, 2003, **119**, 1489–1501.
- 64 R. A. Sultanov and N. Balakrishnan, Quantum mechanical investigations of the $N(^4S) + O_2(X^3\Sigma_g^-) \rightarrow NO(X^2\Pi) + O(^3P)$ reaction, *J. Chem. Phys.*, 2006, **124**, 124321.
- 65 J.-J. Ma, M.-D. Chen, S.-L. Cong and K.-L. Han, Stereodynamics study of the $N(^4S) + O_2(X^3\Sigma_g^-) \rightarrow O(^3P) + NO(X^2\Pi)$ reaction, *Chem. Phys.*, 2006, **327**, 529–535.
- 66 J. He, F. Chen and J. Li, A quasiclassical trajectory study for the $N(^4S) + O_2(X^3\Sigma_g^-) \rightarrow NO(X^2\Pi) + O(^3P)$ reaction on the new $^2A'$ and $^4A'$ potential-energy surfaces, *J. Chem. Phys.*, 2006, **124**, 054303.
- 67 T. K. Mankodi, U. V. Bhandarkar and B. P. Puranik, Cross-sections for $O_2 + N$ system using the QCT method, *Chem. Phys. Lett.*, 2018, **704**, 21–26.
- 68 Y. Wang and X. Cheng, State-to-state transition study of the exchange reaction for $N(^4S)$ and $O_2(X^3\Sigma_g^-)$ collision by quasiclassical trajectory, *J. Phys. Chem. A*, 2021, **125**, 9318–9326.
- 69 J. C. San Vicente Veliz, D. Koner, M. Schwilk, R. J. Bemish and M. Meuwly, The $N(^4S) + O_2(X^3\Sigma_g^-) \rightarrow O(^3P) + NO(X^2\Pi)$ reaction: thermal and vibrational relaxation rates for the $^2A'$, $^4A'$ and $^2A''$ states, *Phys. Chem. Chem. Phys.*, 2020, **22**, 3927–3939.
- 70 Z. Varga, Y. Liu, J. Li, Y. Pauku, H. Guo and D. G. Truhlar, Potential energy surfaces for high-energy $N + O_2$ collisions, *J. Chem. Phys.*, 2021, **154**, 084304.
- 71 A. Caracciolo, J. C. San Vicente Veliz, D. Lu, H. Guo, M. Meuwly and T. K. Minton, Experimental and theoretical studies of hyperthermal $N + O_2$ collisions, *J. Phys. Chem. A*, 2023, **127**, 8834–8848.
- 72 X. Huang, K.-M. Gu, C.-M. Guo and X.-L. Cheng, Dissociation cross sections and rates in $O_2 + N$ collisions: molecular dynamics simulations combined with machine learning, *Phys. Chem. Chem. Phys.*, 2023, **25**, 29475–29485.
- 73 X. Huang and X.-L. Cheng, The role of the sextet potential energy surface in $O_2 + N$ inelastic collision processes, *Phys. Chem. Chem. Phys.*, 2023, **25**, 4929–4938.
- 74 D. L. Baulch, C. J. Cobos, R. A. Cox, G. Hayman, Th Just, J. A. Kerr, T. Murrells, M. J. Pilling, J. Troe, R. W. Walker and J. Warnatz, Evaluated kinetic data for combustion modelling, Supplement I, *J. Phys. Chem. Ref. Data*, 1994, **23**, 847 and references cited therein.
- 75 M. E. Whitson, Jr., L. A. Darnton and R. J. McNeal, Vibrational energy distribution in the NO produced by the reaction of $N(^4S)$ with O_2 , *Chem. Phys. Lett.*, 1976, **41**, 552–556.
- 76 A. Rahbee and J. J. Gibson, Rate constants for formation of NO in vibrational levels $v = 2$ through 7 from the reaction $N(^4S) + O_2 \rightarrow NO^+ + O$, *J. Chem. Phys.*, 1981, **74**, 5143–5148.
- 77 R. R. Herm, B. J. Sullivan and M. E. Whitson, Jr., Nitric oxide vibrational excitation from the $N(^4S) + O_2$ reaction, *J. Chem. Phys.*, 1983, **79**, 2221–2230.
- 78 I. C. Winkler, R. A. Stachnik, J. I. Steinfeld and S. M. Miller, Determination of NO ($v = 0-7$) product distribution from the $N(^4S) + O_2$ reaction using two-photon ionization, *J. Chem. Phys.*, 1986, **85**, 890–899.
- 79 G. E. Caledonia, R. H. Krech, D. B. Oakes, S. J. Lipson and W. A. M. Blumberg, Products of the reaction of 8 km s⁻¹ $N(^4S)$ and O_2 , *J. Geophys. Res.*, 2000, **105**, 12833–12837.
- 80 S. K. Gray and G. G. Balint Kurti, Quantum dynamics with real wave packets, including application to three-dimensional ($J = 0$) $D + H_2 \rightarrow HD + D$ reactive scattering, *J. Chem. Phys.*, 1998, **108**, 950–962.
- 81 A. J. H. M. Meijer, E. M. Goldfield, S. K. Gray and G. G. Balint Kurti, Flux analysis for calculating reaction probabilities with real wave packets, *Chem. Phys. Lett.*, 1998, **293**, 270–276.
- 82 J. Z. H. Zhang, *Theory and Application of Quantum Molecular Dynamics*, World Scientific, Singapore, 1999.
- 83 P. Gamallo, P. Defazio, M. González and C. Petrongolo, Renner-Teller coupled-channel dynamics of the $N(^2D) + H_2$ reaction and the role of the $NH_2 A^2A_1$ electronic state, *J. Chem. Phys.*, 2008, **129**, 244307.
- 84 L. M. Raff and D. L. Thompson, in *Theory of Chemical Reaction Dynamics*, ed. M. Baer, Boca Raton, 1985, vol. 3, pp. 1–121.
- 85 S. Akpınar, I. Armenise, P. Defazio, F. Esposito, P. Gamallo, C. Petrongolo and R. Sayós, Quantum mechanical and quasiclassical Born–Oppenheimer dynamics of the reaction $N_2(X^1\Sigma_g^+) + O(^3P) \rightarrow N(^4S) + NO(X^2\Pi)$ on the $N_2O a^3A''$ and b^3A' surfaces, *Chem. Phys.*, 2012, **398**, 81–89.
- 86 F. Esposito, C. M. Coppola and D. De Fazio, Complementarity between quantum and classical mechanics in chemical modeling. The $H + HeH^+ \rightarrow H_2^+ + He$ reaction: a rigorous test for reaction dynamics methods, *J. Phys. Chem. A*, 2015, **119**, 12615–12626.
- 87 F. J. Aoiz, V. Sáez-Rábanos, B. Martínez-Haya and T. González-Lezana, Quasiclassical determination of reaction probabilities as a function of the total angular momentum, *J. Chem. Phys.*, 2005, **123**, 094101.
- 88 D. C. Chatfield, S. L. Mielke, T. C. Allison and D. G. Truhlar, Quantized dynamical bottlenecks and transition state control of the reaction of D with H_2 . Effect of varying the total angular momentum, *J. Chem. Phys.*, 2000, **112**, 8387–8408.
- 89 N. Zettili, *Quantum Mechanics. Concepts and Applications*, John Wiley and Sons, Chichester, UK, 2022.
- 90 J. M. Bowman, Reduced dimensionality theory of quantum reactive scattering, *J. Phys. Chem.*, 1991, **95**, 4960–4968.

